Bulk Properties of Anharmonic Chains in Strong Thermal Gradients: Non-Equilibrium ϕ^4 Theory

Kenichiro AOKI[a*] and Dimitri KUSNEZOV[b†]

^{a}Dept. of Physics, Keio University, 4—1—1 Hiyoshi, Kouhoku–ku, Yokohama 223–8521, Japan

^{b}Center for Theoretical Physics, Sloane Physics Lab, Yale University, New Haven, CT 06520-8120

ABSTRACT

We study nonequilibrium properties of a one-dimensional lattice Hamiltonian with quartic interactions in strong thermal gradients. Nonequilibrium temperature profiles, $T(x)$, are found to develop significant curvature and boundary jumps. From the determination of the bulk thermal conductivity, we develop a quantitative description of $T(x)$ including the jumps.

* E–mail: `ken@phys-h.keio.ac.jp`

†E–mail: `dimitri@nst4.physics.yale.edu`

The description of transport in physical systems is usually relegated to the near equilibrium regime, where Green-Kubo theory can be used. When one strays from this into systems far from equilibrium, far less is known about the statistical mechanics, or the behavior of transport coefficients [1]. While the physics of non-equilibrium systems is certainly of broad interest, many basic problems have yet to be fully understood. Of particular interest are the non-equilibrium stationary states and the nature of the statistical mechanics which characterize it. One approach to understanding this problems is to place systems in thermal gradients and examine the long time behavior of observables. In one dimension, this has been done in a variety of problems where both finite and divergent transport coefficients were measured. Typically the transport coefficients are found to diverge when the Hamiltonian conserves total momentum. This is typical of systems where the interactions depend only upon differences $x_i - x_j$, such as the FPU and Toda chains [1–3]. When an 'on site' potential, $V(x_i)$, is also present, the coherent propagation of long wavelength modes is suppressed resulting in finite conductivity [4]. This is the case in the Frenkel-Kontorova, ding-a-ling, Lorenz and other models [5–8]. Bulk behavior is also known in higher dimensions as well [9].

In this letter, we investigate the non-equilibrium steady state properties and thermal transport of lattice Hamiltonians with quartic interactions in 1 spatial dimension. Our system is the discrete version of ϕ^4 scalar field theory, a proto-typical field theory that has broad application. In contrast to systems such as the FPU β model [2,4,10], which have divergent thermal conductivities, we find a well defined bulk limit for our non-equilibrium results. This we attribute to the on-site nature of the ϕ^4 interaction. Certain properties of this theory have been studied in the past, which include the Hamiltonian dynamics and phase transitions, as well as the ergodic properties [11]. However, the thermal conductivity has not been determined, and further, there is yet no understanding of the role of boundary jumps and its inter-relation with the shape of the non-equilibrium thermal profile. We present a quantitative analysis of this effect which describes the behavior near and far from thermal equilibrium. A full description of the temperature profiles far from equilibrium is

shown to require a description of the boundary jumps.

Our model system is the 1-dimensional Hamiltonian

$$H' = \frac{1}{2} \sum_{i=1}^{L} \left[\frac{\hat{p}_i^2}{m} + \chi^2(\hat{q}_{i+1} - \hat{q}_i)^2 + \frac{1}{2}\beta^2 \hat{q}_i^4 \right], \tag{1}$$

where β^2, m and χ are parameters. This model becomes identical to the FPU β model if we substitute $(q_{i+1} - q_i)^4$ for q_i^4 in the interaction. It is convenient to perform the rescalings $\hat{q}_i = q_i(\chi/\beta)$, $\hat{p}_i = p_i(\sqrt{m}\chi^2/\beta)$ and $\hat{t} = t(\sqrt{m}/\chi)$. In the dimensionless variables q_i, p_i, t, the Hamiltonian is

$$H = \frac{1}{2} \sum_{i=1}^{L} \left[p_i^2 + (q_{i+1} - q_i)^2 + \frac{1}{2}q_i^4 \right], \tag{2}$$

where $H = H'\beta^2/\chi^4$. To study the statistical mechanics of H in strong thermal gradients, we evolve Hamilton's equations of motion together with thermal boundary conditions on the two ends. Observables are allowed to converge to steady-state values, which are then analyzed. The dynamics is solved on a spatial grid using either fifth and sixth order Runge-Kutta or leap-frog algorithms [12]. We impose time-reversal invariant, thermal boundary conditions on the equations of motion at sites $i = 1$ and $i = L$. Specifically, the endpoint equations are augmented to include dynamical thermal constraints using the robust methods of [13,14], and become:

$$
\begin{aligned}
\dot{q}_1 &= p_1, & \dot{q}_L &= p_L, \\
\dot{p}_1 &= -\frac{\partial H}{\partial q_1} - \frac{a_1}{T_c^0}w_1^3 p_1 - \frac{a_2}{T_c^0}w_2 p_1^3, & \dot{p}_L &= -\frac{\partial H}{\partial q_L} - \frac{a_3}{T_h^0}w_3^3 p_L - \frac{a_4}{T_h^0}w_4 p_L^3, \\
\dot{w}_1 &= a_1(p_1^2/T_c^0 - 1), & \dot{w}_3 &= a_3(p_L^2/T_h^0 - 1), \\
\dot{w}_2 &= a_2(p_1^4/T_c^0 - 3p_1^2) & \dot{w}_4 &= a_4(p_L^4/T_h^0 - 3p_L^2).
\end{aligned}
\tag{3}
$$

The auxiliary variables w_k dynamically implement the statistical boundary conditions consistent with the boundary temperatures T_c^0 and T_h^0 [13]. We will use the optimal choices for the couplings a_i, which in this case are $a_i = 1$ [14]. (We have checked that the results presented here do not depend on this particular choice of the thermostats w_k, the values of a_i, nor on the number of sites at each end that are thermostatted. We have also examined thermostatting from 1 to 3 sites on each end; we return to this point when we discuss

boundary jumps.) With this control of the endpoint temperatures, we are able to simulate the dynamics of H with the boundary thermostat temperatures (T_c^0, T_h^0) fixed. Apart from the endpoints, the system evolves according to the dynamics dictated by the Hamiltonian (2). In the simulations, we use between 10^6 and 10^9 with time steps of dt from 0.1 to 0.001. The lattice size was varied from $L = 10$ to 8000.

In order to understand the transport properties, it is useful to start with the stress-energy tensor $\mathcal{T}^{\mu\nu}$. From the continuity equation,

$$\frac{\partial}{\partial x^\mu} \mathcal{T}^{\mu\nu} = \frac{\partial}{\partial t} E + \nabla J = 0, \tag{4}$$

where $E = \mathcal{T}^{00}$ is the energy density. For thermal gradients in the $x-$direction, we can identify $J = \mathcal{T}^{0x}(x_i, t) = -p_i(q_{i+1} - q_i)$ as the heat flux.

$\underline{T_c^0 = T_h^0}$: By setting $T_c^0 = T_h^0 = T$, we verify that the canonical ensemble is realized at all sites. This is done in several ways. By following the trajectories $p_i(t)$ and histogramming the values at each time step, one reconstructs the entire momentum distribution at any site, which are found to converge to $f(p_i) \propto \exp[-p_i^2/2T]$. We also verify the virial theorem for the kinetic and potential energies.

In thermal equilibrium, we can use the Green-Kubo formula to compute the thermal conductivity $\kappa(T)$ in the linear-response regime:

$$\kappa(T) = \frac{1}{NT^2} \int_0^\infty dt \sum_{k,k'} \langle J(x_k, t) J(x_{k'}, 0) \rangle_{EQ}. \tag{5}$$

The autocorrelation function is evaluated in the canonical ensemble, $T_1^0 = T_2^0$, and the number of points used in the sum is $N < L$ since we omit points near the boundaries. The formula is expected to hold within the linear regime, at least in higher dimensions. In 1-d, the integrand in (5) has been argued to develop a long time tail $\sim t^{-1/2}$ on time scales on the order of a few ten times the mean free time, leading to the divergence of (5) [15]. In our case, the presence of the on site interactions serve to destroy this long-time tail at sufficiently large times. We plot the absolute value of the integrand of (5) for a temperature $T = 1/10$ in Fig. 1 (top). At this temperature the mean free time roughly 50, so that long-time tails

4

should be present on times $\sim 10^3$. The $t^{-1/2}$ behavior is indicated by the dashed line. The time integral is given in 1 (bottom), showing that the integral (5) is finite. These linear response predictions will be seen to agree with the direct measurements we discuss below. We see that on the time scales of $t \sim 50$, there is some agreement with the long-time tail predictions. However, on longer times the divergent behavior is not present, and the linear response results converge to a well defined limit. In Fig. 2, we compile the Green-Kubo measurements of κ, plotted as a function of T. In the context of the FPU model, it has recently been shown that the long-time tails of the autocorrelation function behave as $t^{-3/5}$ leading to a $t^{2/5}$ divergence, based on mode-coupling theory [16]. While we do not have a divergence in our integrals, the behavior of the integrated autocorrelation function in the transient regime is much closer to $t^{1/2}$ at all measured temperatures.

$T_h^0 \gtrsim T_c^0$: We can verify the linear response calculations through a direct measurement of the heat flow. The thermal conductivity κ is defined using Fourier's law $\langle J \rangle_{NE} = -\kappa \partial_x T(x)$, where $\langle J \rangle_{NE}$ is the averaged heat flux. The gradient is evaluated by taking $|T_h^0 - T_c^0|$ sufficiently small so that the temperature profile is linear. We then vary the temperature difference $|T_h^0 - T_c^0|$ around the same average temperature to verify that J is proportional to ∇T, and extract $\kappa(T)$. $T(x)$ is the local temperature defined through an ideal gas thermometer, by $T(x) = \langle p^2(x) \rangle_{NE}$, where $p(x)$ is the momentum at site x. Here $\langle \cdots \rangle_{NE}$ indicates the ensemble average over the non-equilibrium steady state. To obtain the transport properties, each simulation is run long enough for observables such as J, the energy density as well as distribution functions to converge. In Fig. 2 we show the results of both direct measurements and Green-Kubo predictions for κ. We find that both agree over several orders of magnitude, and that $\kappa(T)$ has the power law temperature dependence

$$\kappa(T) = \frac{A}{T^\gamma}, \qquad \gamma = 1.35(2), \qquad A = 2.83(4), \qquad (6)$$

reminiscent of the behavior of lattice phonons at high temperature [17]. We have also verified that a sensible bulk behavior exists, as shown in Fig. 3; the thermal conductivity is independent of L when it is larger than the mean free path, which, on the lattice, is of

order of the conductivity (see below). The dashed lines in Fig. 3 correspond to the values of Eq. (6) at that temperature.

$T_h^0 \gg T_c^0$: By controlling T_c^0 and T_h^0 we can begin to explore the non-equilibrium steady state. For $T_c^0 \sim T_h^0$, we expect to be in the linear regime, with a linear temperature profile, and transport given by Fourier's law. This has been readily verified. As the difference between endpoint temperatures increases, two characteristics emerge: the temperature profile develops curvature (Fig. 4(a) where $T_c^0/T_h^0 = 0.05$), and there are substantial temperature jumps near the boundaries (Fig. 4(c)).

When the temperature varies substantially in the system, one cause for the non–linearity is the temperature dependence of the thermal conductivity. If we assume that the temperature dependence of the thermal conductivity is the dominant source of the non-linearity of the thermal profile, $T(x)$ can be obtained by integrating Fourier's law as

$$T(x) = T_c \left[1 - \left(1 - \left(\frac{T_h}{T_c} \right)^{1-\gamma} \right) \frac{x}{L} \right]^{\frac{1}{1-\gamma}}, \qquad \gamma \neq 1. \tag{7}$$

The integration is simple since the energy flow $\langle J \rangle_{NE}$ is independent of x due to current conservation. This result is distinct from temperature profiles discussed previously as in Ref. [6]. In this equation, the temperatures $T_{c,h}$ denote the temperatures at the boundaries obtained by extrapolating the temperature profile. These are in general different from the endpoint temperatures $T_{c,h}^0$. (In Fig. 4(c), $T_c^0 = 0.05$ and $T_c = 0.096$.) The temperature profile is a function only of x/L so that it has a smooth continuum limit. The ratio of Eq. (7) to the measured local temperature is shown in Fig. 4 (b). Aside from the endpoints, one can see that the agreement is quite good. We have found that this formula works well in higher dimensions as well ($d = 2, 3$) [18].

It is clear that while the formula for $T(x)$ describes the shape of our observed non-equilibrium profiles, it depends on quantities which are not determined from our input parameters, namely the extrapolated temperatures. Hence a complete description of $T(x)$ will require the understanding of how the boundary jump $T_c - T_c^0$ (and similarly for T_h) depends on the parameters of the system. We will do this below.

6

From Eq. (7), we find the heat flux in the non-equilibrium steady state to be

$$\langle J \rangle_{NE} = \frac{A}{L(1-\gamma)}(T_c^{1-\gamma} - T_h^{1-\gamma}).$$ (8)

We can expand this around the average temperature $T_{av} = (T_h + T_c)/2$, to find:

$$\langle J \rangle_{NE} = \langle J \rangle_{NE}^0 \left\{ 1 + \frac{\gamma(\gamma+1)}{24} \left(\frac{\Delta T}{T_{av}} \right)^2 + O\left(\left[\frac{\Delta T}{T_{av}} \right]^4 \right) \right\}, \qquad \langle J \rangle_{NE}^0 = -\kappa(T_{av}) \frac{T_h - T_c}{L}$$ (9)

Here $\langle J \rangle_{NE}^0$ is identified as the constant (temperature) gradient limit of the heat flux, which actually provides a good approximation to the heat flux even when there is curvature in the temperature profile, providing $\Delta T/T_{av} \lesssim 1$. For $\Delta T/T_{av} \sim 1$, the notion of local equilibrium becomes questionable, and this description of the heat flux starts to break down [18].

As we mentioned previously, a common feature to non-equilibrium steady states is the appearance of boundary jumps or slips [4,2,19]. These are not artifacts of the simulation, but are true physical effects [19,20]. For systems in thermal gradients, the boundary temperature can be different from the temperature of the system near the edges. Similar behavior can also appear in fluids which are sheared [21]. In this case there is slippage between the system and the wall. Such effects are well known sources of error in the experimental measurement of the transport coefficients in fluids [20]. In our lattice model, elementary kinetic theory predicts a thermal conductivity of $\kappa = C_V c_s l$ for the system, where C_V is the heat capacity per volume, c_s the sound velocity and l the mean free path. The formula applies to the basic excitations, the "phonons", of the system. In our model, $C_V, c_s \sim 1$. Therefore, the mean free path is expected to be of order of the conductivity itself. This allows us to clarify the nature of the temperature jumps at the boundaries. The jump, arising due to the finite mean free path, satisfies a relation

$$T_i - T_i^0 = \eta \left. \frac{\partial T}{\partial n} \right|_{boundary} = \pm \eta \left. \frac{\partial T}{\partial x} \right|_{boundary}$$ (10)

when $l \ll L$ [19]. Here $\partial T/\partial n$ is the normal derivative at the surface, so that the $+$ $(-)$ sign corresponds to the lower (upper) edge of the chain. We will consider the lower temperature end (the $+$ sign), but identical results hold for the high temperature side if one changes the

sign accordingly. η is expected to behave like the mean free path and hence the conductivity, roughly speaking. If we let $\eta = \alpha \kappa$ for some constant α, we can use Eq. (8) to find the approximate behavior of the boundary jumps:

$$T_c - T_c^0 \simeq \alpha \langle J \rangle_{NE} \tag{11}$$
$$\sim (T_h^0 - T_c^0)\frac{\alpha \kappa(T_{av})}{L} + \cdots.$$

We have determined η by fitting Eq. (7) to profiles $T(x)$ obtained from various non–equilibrium steady states, using the power γ obtained from Eq. (6). The behavior of η as a function of T from the non–linear thermal profiles is plotted in Fig. 5 (top), which can be fitted to $\eta = (6.1 \pm 0.5) \times T^{-1.5 \pm 0.1}$, consistent with the above argument. We can also use (11) to study the boundary jumps directly. In Fig. 5 (bottom), we see that Eq. (11) is readily verified in the data, which includes thermal profiles both near and far from equilibrium. A simple fit (dashes) provides the coefficient $\alpha = 2.6(1)$, fully consistent with $\eta(T) = \alpha \kappa(T)$. We have analyzed these effects in higher dimensions as well and find similar results [18].

We now have the following behavior: Thermal boundary conditions will result in a given amount of heat flux, which in turn determines the magnitude of the boundary jumps through Eq. (11). Once the boundary jumps are defined, the thermal profile, Eq. (7), is determined from the endpoint temperatures T_i^0. We have examined the dependence of the results we present here on the types of thermal boundary conditions we have used. This includes variations not only of the strengths of the interactions, a_i, but also of the number of thermostatted sites on each end. We have observed that the coefficient α (and hence η) is not a physical property of the Hamiltonian, but can depend on the thermostats. Different thermostats can produce different boundary jumps for the same boundary temperatures $T_{c,h}^0$. Although the new jumps provide new extrapolated temperatures $T_{c,h}$, the temperature profile is still predicted by Eq. (7). Hence the formulas we have presented are still valid in spite of the (slight) differences in boundary jumps. These differences do not lead to any modification of the transport coefficients, and are only differences in the shape $T(x)$ due to

the variation of the boundary jumps which seem to reflect the efficiency at which heat can be transfered to the system through the boundary in the far from equilibrium regime.

We have constructed the non-equilibrium steady states of an anharmonic chain with quartic interactions, by placing it in strong thermal gradients, and obtained well defined bulk transport properties. These results are also valid for classical ϕ^4 lattice field theory. We determined the temperature dependence of the thermal conductivity, and then derived the non-equilibrium thermal profile $T(x)$, which agrees well with the observed behavior in the non-equilibrium steady state. A simple expression for the non-equilibrium heat flux is also found to agree well with direct measurements. Using these results, as well as arguments from kinetic theory, we are able to quantify the temperature jumps at the edges of our system, which are endemic to both non-equilibrium simulations and experiment. We hope to develop this overall picture of the non-equilibrium steady state towards understanding the dynamics of phase transitions under non-equilibrium conditions, as well as the concepts of local equilibrium.

REFERENCES

[1] W.G.Hoover, *Computational Statistical Mechanics* (Elsevier, Amsterdam, 1991); D.J.Evans, G.P.Morriss, *Statistical Mechanics of Non-Equilibrium Liquids* (Academic, London, 1990); P. Gaspard, *Chaos, Scattering and Statistical Mechanics*, (Cambridge, New York, 1998); J.P.Eckmann, C. Piller, L. Bellet, *Comm. Math. Phys.* **201** (1999) 657.

[2] S. Lepri, R. Livi, A. Politi, *Phys. Rev. Lett.* **78** (1997) 1896; H. Kaburaki, M. Machida, *Phys. Lett.* **A181** (1993) 85.

[3] M. Mareschal, A. Amellal, *Phys. Rev.* **A37** (1988) 2189.

[4] T. Hatano, *Phys. Rev.* **E59** (1999) R1; T. Tanenbaum, G. Ciccotti, R. Gallico, *Phys. Rev.* **A25** (1982) 2778.

[5] M.J. Gillian, R.W. Holloway, *J. Phys.* **C18** (1985) 5705; B. Hu, B. Li, H. Zhao, *Phys. Rev.* **E57** (1998) 2992; F. Mokross, H. Büttner, *J. Phys.* **C16** (1983) 4539.

[6] D.J.R. Mimnagh, L.E.Ballentine, *Phys. Rev.* **E56** (1997) 5332; D. Alonso, R. Artuso, G. Casati, I. Guarneri, *Phys. Rev. Lett.* **82** (1999) 1859.

[7] G. Casati, J. Ford, F. Vivaldi, W.M. Visscher, *Phys. Rev. Lett.* **52** (1984) 1861; H. Posch, W.G.Hoover, *Phys. Rev.* **E58** (1998) 4344.

[8] S. Takesue, *Phys. Rev. Lett.* **64** (1990) 252; T. Prosen, M. Robnik, *J. Phys. A* **25** (1992) 3449.

[9] See, for instance, R.H.H. Poetzsch, H. Böttger, *J. Phys. Cond. Matt.* **10** (1998) 943; C. Oligschleger, J.C. Schön, *Phys. Rev.* **B** (1999) 4125.

[10] J. Ford, *Phys. Rep.* **213** (1992) 271.

[11] L. Caiani, L. Casetti, M. Pettini, *J. Phys. A: Math. Gen.* **31** (1998) 3357; L. Caiani *et al*, *Phys. Rev.* **E57** (1998) 3886; G. Parisi, *Europhys. Lett.* **40** (1997) 357.

[12] See, for instance, W.H. Press, B.P. Flannery, S.A. Teukolsky, W.T. Vetterling, *Numerical Recipes*, (Cambridge Univ. Press, New York, 1992).

[13] D. Kusnezov, A. Bulgac, W. Bauer, *Ann. Phys.* **204** (1990) 155; D. Kusnezov, *Phys. Lett.* **166A** 315 (1992).

[14] D. Kusnezov, J. Sloan, *Nucl. Phys.* **B409** (1993) 635; D. Kusnezov, *Phys. Lett.* **289B** 395 (1992).

[15] J.R. Dorfman, E.G.D. Cohen, *Phys. Rev. Lett.* **25** (1970) 1257; M.H. Ernst, E.H. Hauge, J.M.J van Leeuwen, *Phys. Rev. Lett.* **25** (1970) 1254, *Phys. Rev.* **A** 1971 2055; Y. Pomeau, P. Résibois, Phys. Rev. C **19** (1975) 63 and references therein.

[16] S. Lepri, R. Livi, R. Politi, *Europhys. Lett.* **43** (1998) 271.

[17] C. Herring, *Phys. Rev.* **95** (1954) 954.

[18] K. Aoki and D.Kusnezov, preprint.

[19] E. M. Lifshits, L.P. Pitaevskii, *Physical Kinetics*, (Pergamon Press, New York, 1981).

[20] See, for instance, H. Ziebland, in *Thermal Conductivity*, ed. R. P. Tye, (Academic, New York, 1969), Vol 2.

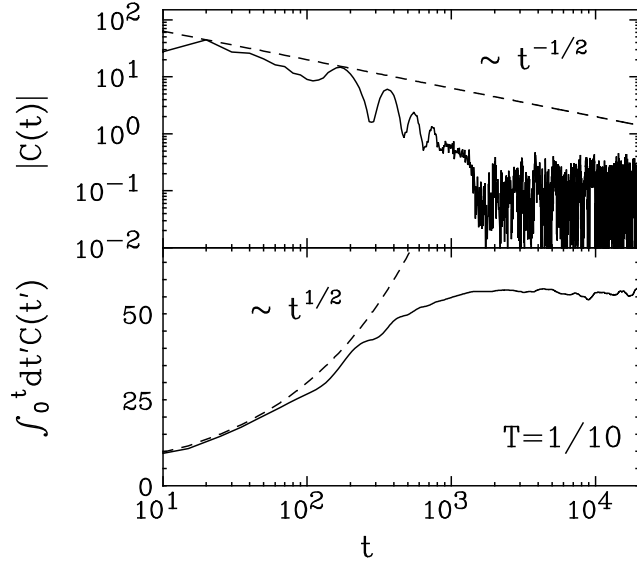[21] D.K.Bhattacharya and G.C.Lie, *Phys. Rev. Lett.* **62** (1989) 897.

FIG. 1. (Top) Absolute value of the autocorrelation function $C(t) = \sum_{k,k'} \langle J(x_k, t) J(x_{k'}, 0) \rangle_{EQ} / NT^2$, for $L = 100$, up to a time $t = 2 \times 10^4$. The long-time tail divergence would have the behavior shown by the dashed line. (Bottom) Green-Kubo integral up to time t, showing convergence of κ. The dashed line is the anticipated behavior if the long-time tail divergence were present. One can see that on the time scales $t \sim 10^3$ (a few ten times the mean free time), similar behavior can be seen, although it vanishes for larger times.
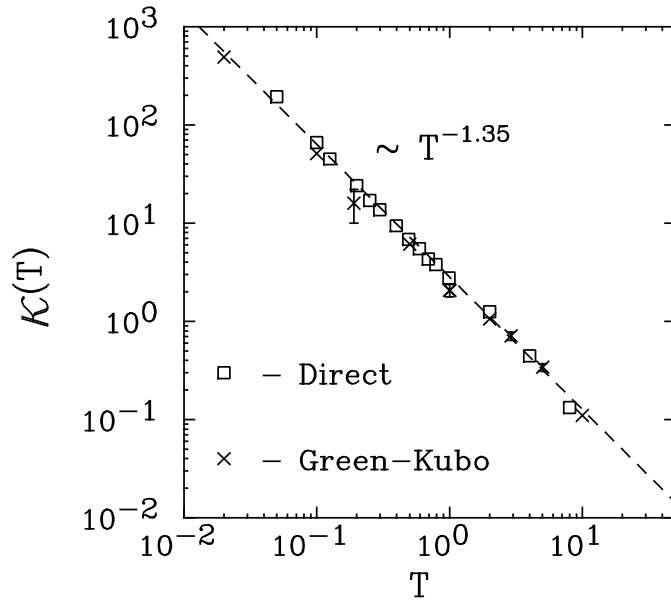
FIG. 2.   Thermal conductivity κ obtained from direct ($\square$) and Green-Kubo ($\times$) measurements for various lattice sizes L, and the power law fit $\kappa(T) = 2.83(4)/T^{1.35(2)}$ (dashes).   Green-Kubo integrals readily converge to values consistent with direct measurements.
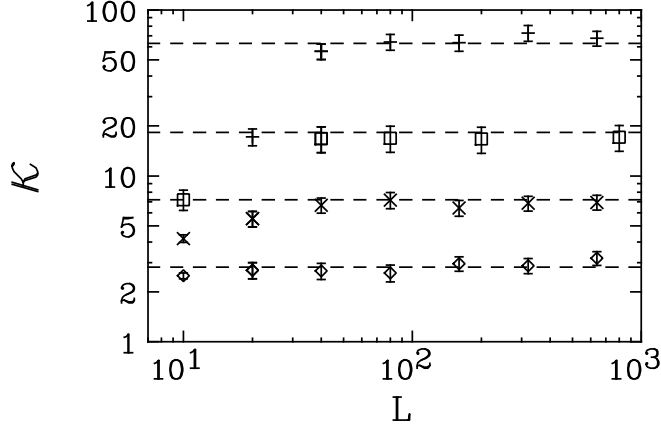

FIG. 3.   Size (L) dependence of the thermal conductivity indicating bulk behavior, for temperatures (upper to lower) $T = 1/10$ (+), $1/4$ ($\square$), $1/2$ ($\times$) and 1 ($\diamond$).   The dashed lines are the predictions from Eq. (6) for that temperature.
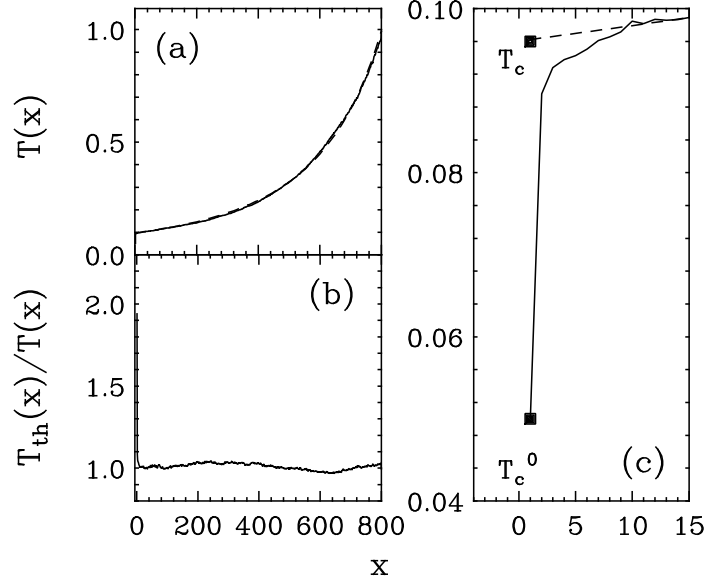
FIG. 4.   (a) Non-equilibrium therm al profile $T(x)$ as a function of position (solid), compared to theoretical predictions of Eq. (7) (dashes) which lie on the solid curve. The temperature was sampled 10^6 times every $\Delta t = 0.25$. Endpoints were thermalized at $(T_c^0, T_h^0) = (0.05, 1)$. (b) The ratio of the predicted profile, Eq. (7), to that measured in (a). Aside from the boundary jumps, the agreement is within a few percent. (c) Blowup of the temperature jumps at the low end of (a). The simulated temperature T_c^0 can differ significantly from the extrapolated value T_c.
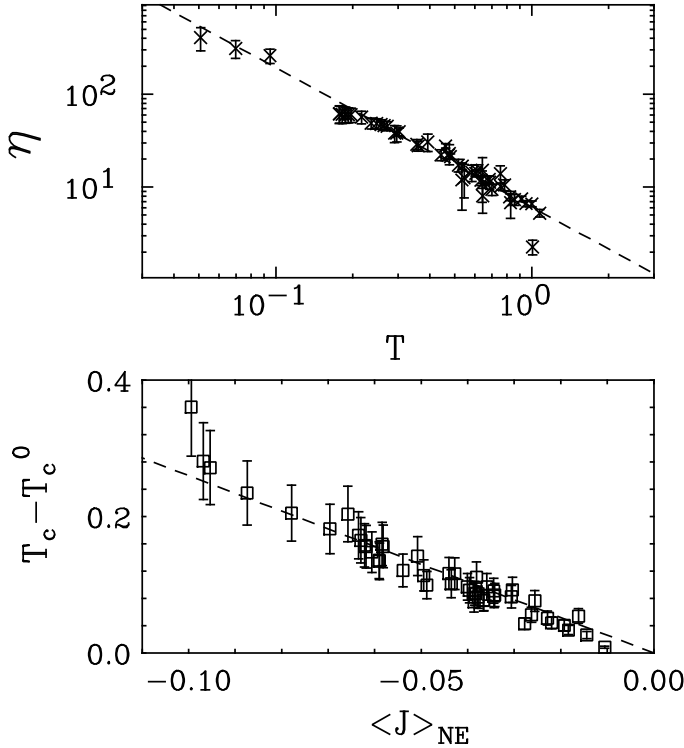

FIG. 5. (Top) Temperature dependence of the jump parameter η and its approximate power law behavior (dashes). (Bottom) Verification of Eq. (11). We plot the measured boundary jumps as a function of the non-equilibrium heat flux. The slope provides the coefficient $\alpha = 2.6(1)$ which relates η to the conductivity κ via $\eta = \alpha\kappa$.